J Arid Land (2025) 17(4): 481–499
doi: 10.1007/s40333-025-0097-4; CSTR: 32276.14.JAL.02500974

Science Press Springer-Verlag

Spatiotemporal variations and driving mechanisms of flash droughts during 1981–2020 in the Qilian Mountains, China

BAI Junhong[1,2], WANG Jianglin[1*], CHEN Jie[3], WANG Xuejia[3]

[1] Key Laboratory of Ecological Safety and Sustainable Development in Arid Lands, Northwest Institute of Eco-Environment and Resources, Chinese Academy of Sciences, Lanzhou 730000, China;
[2] University of Chinese Academy of Sciences, Beijing 100049, China;
[3] Key Laboratory of Western China's Environmental Systems (Ministry of Education), College of Earth and Environmental Sciences, Lanzhou University, Lanzhou 730000, China

Abstract: Flash drought is characterized by a period of rapid drought intensification with impacts on agriculture, water resources, ecosystems, and human environment. In the Qilian Mountains, northwestern China, flash droughts are becoming more frequently due to the global climate warming. However, the spatiotemporal variations and their driving factors of flash droughts are not clear in this region. In this study, the European Centre for Medium-range Weather Forecasts (ECMWF) Reanalysis v5-Land (ERA5-Land) dataset was utilized to identify two types of flash drought events (heatwave-induced and water scarcity-induced flash drought events) that occurred in the growing season (April–September) during 1981–2020 in this area. The results showed that the frequency of heatwave-induced flash droughts has decreased since 2010, while the frequency of water scarcity-induced flash droughts has declined markedly. Spatially, heatwave-induced flash droughts were predominantly concentrated in the western Qilian Mountains, whereas water scarcity-induced flash droughts were primarily concentrated in the central and eastern Qilian Mountains. A significantly increasing temporal trend in both types of flash droughts in the eastern Qilian Mountains was found. Meanwhile, there was a decreasing temporal trend of heatwave-induced flash droughts in the southwestern part of the region. Additionally, the influence of two major atmospheric modes, i.e., the El Niño–Southern Oscillation (ENSO) and North Atlantic Oscillation (NAO), on these two types of flash droughts was explored by the Superposed Epoch Analysis. The ENSO mainly influences flash droughts in the central and eastern parts of the Qilian Mountains by altering the strength of the East Asian monsoon, while the NAO mainly affects flash droughts in the entire parts of the Qilian Mountains by inducing anomalous westerlies activity. Our findings have important implications for predicting the evolution of flash drought events in the Qilian Mountains region under continued climate warming.

Keywords: heatwave-induced flash drought; water scarcity-induced flash drought; El Niño–Southern Oscillation (ENSO); North Atlantic Oscillation (NAO); Superposed Epoch Analysis (SEA); wavelet coherence

Citation: BAI Junhong, WANG Jianglin, CHEN Jie, WANG Xuejia. 2025. Spatiotemporal variations and driving mechanisms of flash droughts during 1981–2020 in the Qilian Mountains, China. Journal of Arid Land, 17(4): 481–499. https://doi.org/10.1007/s40333-025-0097-4; https://cstr.cn/32276.14.JAL.02500974

*Corresponding author: WANG Jianglin (E-mail: wangjianglin2011@lzb.ac.cn)
Received 2024-12-09; revised 2025-03-18; accepted 2025-04-03

1 Introduction

Drought is a climatological phenomenon characterized by a prolonged period of anomalously low precipitation, persisting over varying temporal scales (days, months, or years) and resulting in hydrological deficits and reduced water availability in affected regions (Otkin et al., 2013). Such hydrological deficits impact local soil environments and aquatic systems, and can then adversely affect local agriculture and economic activity, including human livelihoods (Sheffield et al., 2012). There are various classifications of drought, including hydrological drought, agricultural drought, meteorological drought, and socioeconomic drought (Mishra and Singh, 2010). The impacts of drought can be extensive and severe; many regions around the world, such as Sub-Saharan Africa and Australia, frequently experience long-term droughts that last several years or even decades (Zhang et al., 2021b; Ayugi et al., 2022). Meanwhile, areas such as California in the United States, parts of Europe, and northern China often face seasonal and short-term drought events (Spinoni et al., 2018).

With ongoing climate change, the frequency and intensity of extreme weather phenomena are increasing globally (Diffenbaugh et al., 2017; Shenoy et al., 2022). Increases in temperature directly enhance atmospheric evaporation rates, accelerating the loss of terrestrial water and exacerbating existing drought conditions (Zhao et al., 2024). Global warming also alters precipitation patterns, leading to a decrease in rainfall and uneven rainfall distribution across different regions, further intensifying the occurrence and development of droughts (Dai et al., 2018). Additionally, the complexity of the global climate system may result in some regions simultaneously experiencing droughts along with other extreme weather events such as heatwaves, heavy rainfall, or floods (Hoover et al., 2022). When multiple extreme events occur simultaneously in space and time, their cumulative impact can be markedly amplified, greatly surpassing the effects of any individual event (Zscheischler et al., 2018; Raymond et al., 2020). Changes in climate can have profound effects on the spatiotemporal distribution of droughts, potentially transforming what were once single drought events into multifaceted composite drought events. This transformation, creating what are known as compound extreme droughts, is characterized by its unpredictability, complex causative mechanisms, and potential destructiveness, making it a focal point of current research. The term "flash drought" is now commonly used to denote sudden and volatile drought events (Svoboda et al., 2002). This type of drought event can lead to widespread and devastating ecological and socioeconomic impacts (Gazol and Camarero, 2022; Tabari and Willems, 2023).

Currently, research on flash droughts spans different spatiotemporal scales, wherein the characteristics of such events are analyzed at these specific scales. For example, Neelam and Hain (2024) conducted an analysis of flash drought characteristics at a global watershed scale during 1980–2019, emphasizing the spatiotemporal dynamics of flash droughts across diverse watersheds, particularly focusing on their initiation, duration, and spatial coverage. Shi et al. (2024) analyzed flash drought events across different climatic sub-regions of China, with a focus on the interaction between flash droughts and heatwaves; and they demonstrated that the interconnectivity of such events amplifies the frequency, severity, and persistence of extreme phenomena, underscoring the potential hazards posed to ecosystems and socioeconomic systems by compound events. Řehoř et al. (2024) conducted a detailed analysis of flash drought events in central Europe during 1961–2021; and they adopted rigorous criteria to define flash droughts and thoroughly investigated the major atmospheric circulation types responsible for triggering these events. Alizadeh et al. (2020) studied the spatiotemporal evolution of flash drought–heatwave compound events in the United States over the past century, emphasizing the increasing risks posed by the synergistic effects of multiple extreme climatic phenomena. O and Park (2024) analyzed the responses of ecosystems in different climate and vegetation regions worldwide to flash droughts during 2001–2020, emphasizing how flash droughts disrupt ecosystems by affecting the water absorption, photosynthesis, and evapotranspiration capacity of vegetation. Yao et al. (2022) analyzed the effects of flash droughts on vegetation photosynthesis and carbon cycle,

highlighting a decline in the gross primary productivity of vegetation. This decline in primary productivity leads to reduced ecosystem output, thereby disturbing the ecological equilibrium and compromising ecosystem stability. However, research on the identification and characterization of the two different types of flash droughts (i.e., heatwave-induced flash drought and water scarcity-induced flash drought) remains limited, especially in western China.

Moreover, numerous scholars have conducted systematic research on the formation mechanisms and impacts of flash droughts, with particular emphasis on the effects of two atmospheric circulation modes, i.e., the El Niño–Southern Oscillation (ENSO) and North Atlantic Oscillation (NAO). Existing research indicates that atmospheric oscillations during their peak winter phase, especially the ENSO and NAO, usually impact regional droughts in the following summer (Ogi et al., 2003; Chen and Jin, 2020; Xing et al., 2024). Vicente-Serrano et al. (2017) conducted a multiscale analysis of compound drought events in different regions of Ecuador, thoroughly exploring the influence of the ENSO on the spatiotemporal variability of flash droughts in the area; and they found the marked impact of different positive (El Niño) and negative (La Niña) phases on regional drought severity over different time scales. Park et al. (2020) identified a positive correlation between the ENSO and east African climate, where the El Niño phase enhances precipitation and reduces drought events, whereas the La Niña phase induces drier conditions, intensifying drought severity. Similarly, López-Moreno and Vicente-Serrano (2008) found that the positive phase of the NAO generally induces drought in southern Europe and enhances precipitation in northern Europe, whereas the negative phase results in increased rainfall in southern Europe and drier conditions in northern Europe.

Diverse geography and climate across China contribute to pronounced regional heterogeneity in flash drought events. Current research indicates that northwestern, southwestern, and northeastern China, as well as the Yellow River Basin, are hotspots of flash droughts, with northwestern and northeastern events exhibiting greater intensity and persistence (Fu and Wang, 2022; Gong et al., 2022). Temporally, flash drought peaks predominantly occur from late spring to summer, while a secondary peak emerges in September–October in northwestern regions (Hu et al., 2024; Xue et al., 2024). The Qilian Mountains, serving as an ecological corridor between the Loess Plateau and Xizang Plateau and housing the headwaters of major rivers, host a climate-sensitive ecosystem vulnerable to drought-induced ecological disturbances under warming conditions (Nogués-Bravo et al., 2007; Zhang et al., 2021a; Bai et al., 2023). Most previous studies, such as Wang et al. (2021) and Zhou et al. (2024), on flash droughts have focused on the whole of China or Xizang Plateau, while investigations on the influence of atmospheric circulation modes on flash droughts remain lacking. Consequently, research gaps persist regarding localized flash drought dynamics and compound events in the Qilian Mountains. Urgent systematic investigation is required to elucidate drought typologies, driving mechanisms, and atmospheric teleconnections (e.g., ENSO and NAO) in this region. Such efforts are critical to improve early-warning systems, mitigate socioeconomic risks, and develop climate-adaptive conservation strategies. This study aims to identify flash drought events in the Qilian Mountains from 1980 to 2020, analyze their spatiotemporal variations, and explore their relationships with the ENSO and NAO. Our findings will contribute to a better understanding of the regional occurrence patterns of flash droughts and help to prevent ecological and environmental issues related to flash droughts under a future warming climate scenario.

2 Materials and methods

2.1 Study area

The Qilian Mountains (36°43′–39°42′N, 94°24′–103°46′E) are situated in northwestern China, spanning the northeastern part of Qinghai Province and western border of Gansu Province, and extending for approximately 800 km. Positioned deep inland and far from the ocean, this region belongs to the inland arid and semi-arid climate zone, characterized by a typical continental climate with low annual precipitation, which predominantly occurs in summer (Lan et al., 2003;

Bai et al., 2023). The region has a complex topography, featuring high mountains, deep valleys, and basins. In the central and western parts of the Qilian Mountains, the elevation is relatively high, generally ranging from 3500 to over 6000 m; the eastern part has a lower elevation, with altitudes below 3000 m. This topography adds to the complexity and severity of the regional climate and hydrological conditions. Geographically, the Qilian Mountains are located on the northeastern margin of the Xizang Plateau, lying at the confluence of the mid-latitude westerlies and East Asian monsoon belt (Fig. 1) (Huang et al., 2023; Li and Peng, 2023). The moist air brought by the westerlies rises over the windward slopes of the mountains, causing precipitation, while the leeward slopes are relatively dry. However, the influence of the East Asian summer monsoon on the Qilian Mountains is limited because moist air masses reach the eastern part of the region and the strength of the monsoon gradually weakens with the increased elevation.

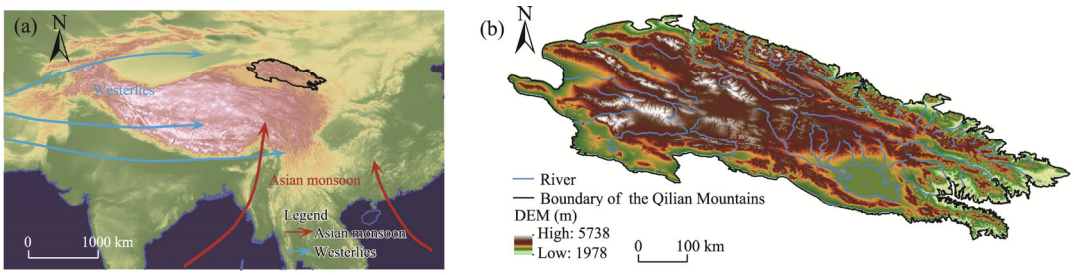

Fig. 1 Wind field (a) and landforms (b) of the Qilian Mountains. The maps used in this study were sourced from the Resource and Environmental Science Data Platform (https://www.resdc.cn/data.aspx?DATAID=123) and the ASTER Global Digital Elevation Model (https://www.jspacesystems.or.jp/ersdac/GDEM/E). DEM, digital elevation model.

2.2 Data

This study utilized the European Centre for Medium-range Weather Forecasts (ECMWF) Reanalysis v5-Land (ERA5-Land) reanalysis dataset (https://cds.climate.copernicus.eu). The ERA5-Land dataset provides a detailed view of surface-variable changes over several decades, at a higher resolution than does ERA5. The dataset is produced by rerunning the land component of the ECMWF ERA5 climate reanalysis and has a temporal resolution of 1 h and spatial resolution of 9 km on a condensed Gaussian grid (TCo1279). Data from the Climate Data Store (CDS) is re-gridded to a standard 0.1°×0.1° latitude–longitude grid. This dataset has been used previously by numerous scholars, yielding robust research outcomes, thus demonstrating its reliability. For example, Zou et al. (2022) analyzed its performance in terms of air temperature in the coastal urban agglomeration of southeastern China; Zha et al. (2023) utilized the dataset to examine the characteristics and trends of flash drought occurrences in the Pearl River Basin of southern China; and Wei et al. (2023) used the dataset to analyze the spatiotemporal variations of temperature in the Qilian Mountains. Herein, we utilized three ERA5-Land climatic variables, i.e., skin temperature, evaporation from bare soil, and volumetric soil moisture. Volumetric soil moisture was assessed across four vertical layers: 0–7, 7–28, 28–100, and 100–289 cm. Given that the majority of vegetation roots are concentrated within the top 100 cm of soil (Jackson et al., 1997), volumetric soil moisture within this depth range directly impacts plant water uptake and growth. This upper soil layer generally exhibits short-term but significant effects on vegetation, and shallow soil moisture changes are more sensitive to short-term variations in precipitation and evaporation, allowing for a timelier assessment of drought onset and development (Seneviratne et al., 2010). Therefore, we focused on volumetric soil moisture data from the top three layers noted above, ensuring reliable data acquisition. Additionally, temperature and precipitation data for this study were accessed from the National Climate Center (https://data.cma.cn). The temperature and precipitation data during 1981–2017 were used in this study, excluding 2018–2020 due to incomplete station coverage.

The ENSO index was obtained from the National Oceanic and Atmospheric Administration (NOAA; https://psl.noaa.gov/data/climateindices/list), while NAO index data were obtained from the National Centers for Environmental Information (NCEI; https://www.ncei.noaa.gov/access/monitoring/nao).

2.3 Definitions of flash drought events

Methods for defining flash droughts are highly diverse and comprehensive. In this study, we integrated and refined the method proposed by Wang and Yuan (2018) to identify flash drought events. We identified flash drought events based on three hydrological indicators, i.e., temperature, evapotranspiration, and soil moisture. We classified flash droughts into two primary categories based on their dominant drivers, i.e., heatwave-induced flash drought and water scarcity-induced flash drought. The classification method based on the aforementioned indicators evaluates drought conditions from multiple perspectives, making it effective in identifying droughts under different climatic conditions.

Using the ERA5-Land dataset, we first extracted hourly temperature, evapotranspiration, and soil moisture data during the warm-season (April–September) during 1981–2020 across the Qilian Mountains. The season-length selected herein follows the criteria used by most researchers in flash drought studies (Zhang et al., 2024; Ma and Yuan, 2025) and also corresponds to the growing season (April–September) in the Northern Hemisphere (Mo and Lettenmaier, 2015). Starting in April, temperatures in the Northern Hemisphere gradually rise, daylight hours increase, and soil temperatures begin to rise accordingly. This continues until September, when temperatures decrease, daylight hours shorten, and soil temperatures start to drop or even freeze. Because our soil moisture data were attained from multiple depth layers, these layers required synthesis for comprehensive analysis. Specifically, according to the actual condition of plant water uptake, we adopted the soil moisture data from the top three layers (0–7, 7–28, and 28–100 cm) of the ERA5-Land dataset, which provides soil moisture at four depths (0–7, 7–28, 28–100, and 100–289 cm). Owing to a lack of detailed soil characteristic data, we assigned soil moisture weights according to the soil layer thickness. Soil moisture content between 0 and 1 m was calculated by summing the moisture content for each layer and weighting it by the thickness of the layer (Zhong et al., 2023). The weights assigned to these layers were 0.07, 0.21, and 0.72, respectively, representing the relative contributions of each depth layer to the overall soil moisture profile. By applying weighted averaging, we consolidated the soil moisture information from different depths into a single composite indicator, facilitating further analysis. Following the weighting of soil moisture data, we aggregated the hourly temperature, evapotranspiration, and soil moisture data into 5-d intervals (Wang and Yuan, 2018). This step converts high-frequency data into a more manageable temporal scale, allowing long-term trends and patterns to be captured, and enhances the stability and reliability of subsequent trend analysis. Finally, using the processed 5-d interval data, we identified and classified flash drought events. This step involves assessing the frequency and intensity of such events.

To determine whether an event was normal or featured anomalously high temperatures, we took one standard deviation from the mean temperature anomaly for the given period as the threshold. To assess abnormally high temperature events or flash drought events, we used the 30^{th} percentile of the soil moisture data as the threshold condition. This percentile was chosen to represent the lower end of the soil moisture distribution, indicating unusually dry conditions (Wang et al., 2018). Additionally, we analyzed the evapotranspiration anomaly, which was compared against its historical average to classify flash drought events. A positive evapotranspiration anomaly suggests that a drought may be heatwave-induced, while a negative anomaly points to water scarcity being the primary driver. This dual mechanism ensures a comprehensive evaluation of drought types, incorporating both temperature and moisture conditions to accurately characterize and understand drought events.

The two types of flash drought events were identified by the following criteria (Fig. 2): type I (heatwave-induced flash drought): $T_{ano}>T_{std}$, $SM_q<30\%$, and $ET_{ano}>0$; and type II (water scarcity-induced flash drought): $T_{ano}>T_{std}$, $SM_q<30\%$, and $ET_{ano}<0$, where T_{ano} is the temperature anomaly (K); T_{std} is the standard deviation of temperature anomaly (K); SM_q is the soil moisture within a specific 5-d period (%); and ET_{ano} is the evapotranspiration anomaly (mm/d).

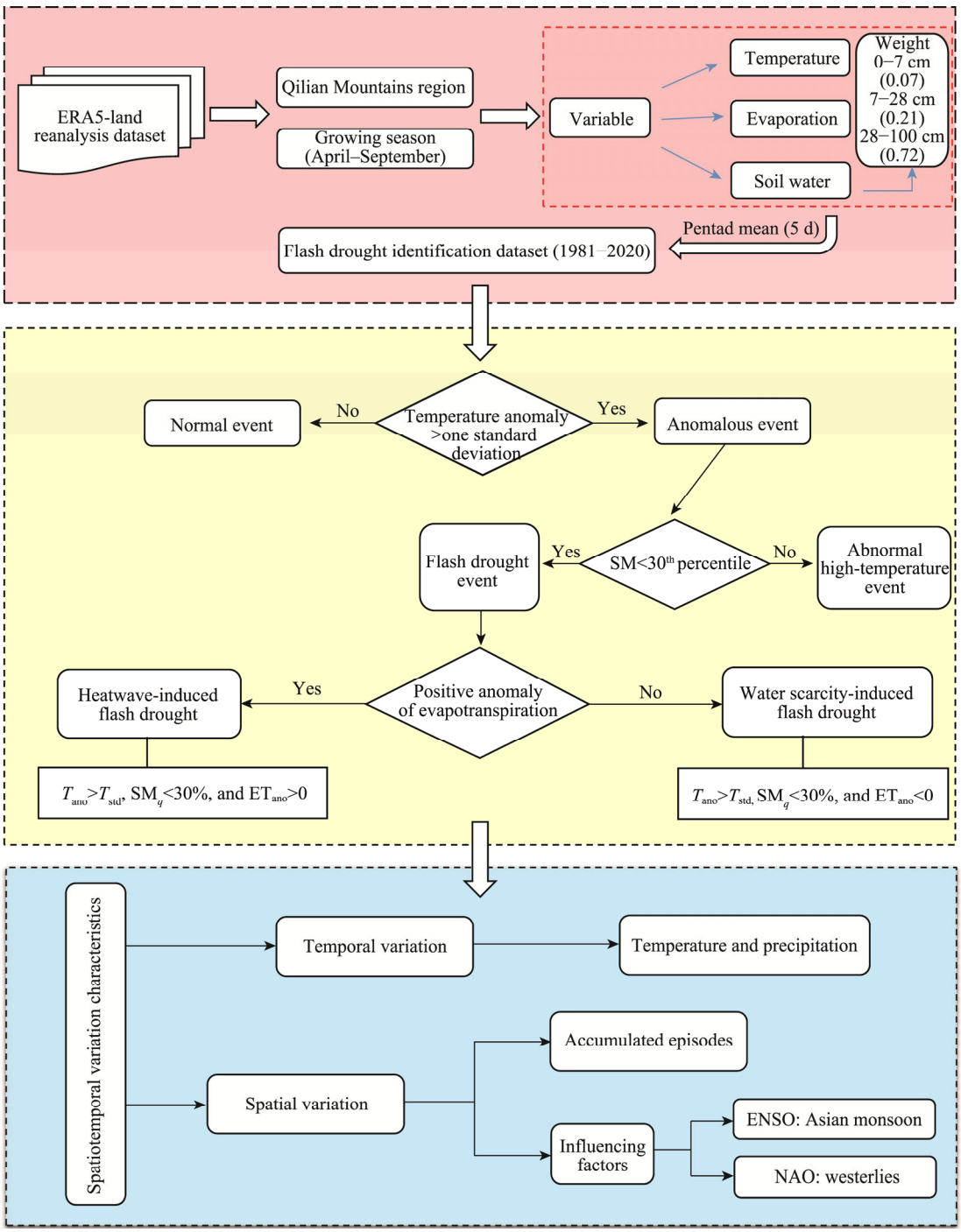

Fig. 2 Identification processes for the two types of flash drought events as well as their spatiotemporal variations. T_{ano}, temperature anomaly value; T_{std}, standard deviation of temperature anomaly; SM_q soil moisture within a specific 5-d period; ET_{ano}, evapotranspiration anomaly value; ENSO, El Niño–Southern Oscillation; NAO, North Atlantic Oscillation.

2.4 Theil-Sen median trend analysis and Mann-Kendall (MK) trend test

The Theil-Sen median trend analysis, also referred to as the Theil-Sen estimator, is a robust approach used to estimate the slope of a trend line in bivariate data. The method is particularly suited to linear trends and offers relatively fast computation, especially with modern tools, making it an efficient choice for trend analysis. The calculation formula is as follows (Jiang et al., 2015):

$$\beta = \text{Median}\left(\frac{x_j - x_i}{j - i}\right), \forall j > i, \tag{1}$$

where β is the Theil-Sen trend slope, representing the median rate of change in the data sequence; Median is the median function; and x_i and x_j are the flash drought identification data at the grid point for years i and j, respectively. If $\beta>0$, the cumulative number of flash drought days is increasing; if $\beta=0$, the cumulative number of flash drought days remains stable; and if $\beta<0$, the cumulative number of flash drought days is decreasing.

The MK trend test is a non-parametric method for assessing trends in time series. It does not require the measurements to follow a normal distribution and is robust to missing values and outliers, making it suitable for detecting significant trends within time series (Li et al., 2021). The test statistic S for the MK test is calculated as follows (Hamed and Ramachandra Rao, 1998; Güçlü, 2020):

$$S = \sum_{i=1}^{n-1} \sum_{j=i+1}^{n} \text{sgn}\left(x_j - x_i\right), \tag{2}$$

where S represents the MK statistics, reflecting the consistency of increasing and decreasing trends in the data sequence; n is number of observations in the time series; and sgn $(x_j - x_i)$ is the sign function, which is defined as follows (Hamed and Ramachandra Rao, 1998; Güçlü, 2020):

$$\text{sgn}\left(x_j - x_i\right) = \begin{cases} 1 & \left(x_j - x_i\right) > 0 \\ 0 & \left(x_j - x_i\right) = 0 \\ -1 & \left(x_j - x_i\right) < 0 \end{cases}, \tag{3}$$

$$W = \begin{cases} \dfrac{S-1}{\sqrt{\text{Var}\left(S\right)}} & S > 0 \\ 0 & S = 0 \\ \dfrac{S+1}{\sqrt{\text{Var}\left(S\right)}} & S < 0 \end{cases}, \tag{4}$$

where W is the standardized value of the test statistic.

The variance is given by (Hamed and Ramachandra Rao, 1998; Güçlü, 2020):

$$\text{Var}\left(S\right) = \frac{n\left(n-1\right)\left(2n+5\right)}{18}. \tag{5}$$

This approach works well for long-term time series data because the use of MK trend test combined with the Theil-Sen median trend analysis provides unmatched benefits over conventional univariate linear regression analysis techniques (Adib et al., 2024). Under a standard normal distribution, at 90%, 95%, and 99% confidence levels, the trend passes the significance test when the absolute value of W is greater than 1.65, 1.96, and 2.58, respectively (Hamed and Ramachandra Rao, 1998).

2.5 Composite analyses for the responses to the anomalous years of ENSO and NAO

We first identified cases (i.e., events) of ENSO and NAO indices during extreme anomalous years during 1981–2020 (López-Moreno and Vicente-Serrano, 2008; Vicente-Serrano et al., 2017; Dogar and Sato, 2018). We then averaged the ENSO and NAO indices for December, January, and February to determine winter season values. Next, we detrended the time series to eliminate

the influence of long-term trends and applied the *Z*-score normalization method to standardize the data. The *Z*-score standardizes data points by measuring their distance from the mean in terms of standard deviations. On the basis of these normalized time series, we selected event years. Years with a *Z*-score>1 were selected as positive event years, while those with a *Z*-score< –1 were selected as negative event years (Fig. 3; Table 1).

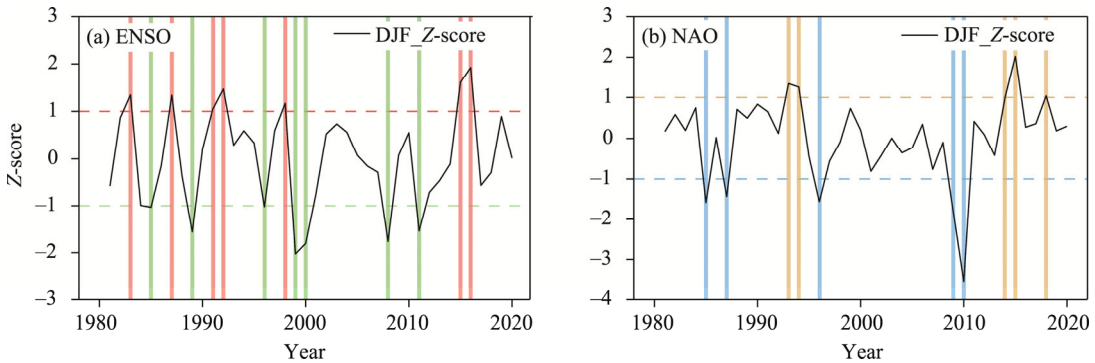

Fig. 3 Normalized time series of ENSO (a) and NAO (b) indices in December-January-February (DJF) during 1981–2020. Red and green bars represent positive and negative ENSO anomaly years, respectively; yellow and blue bars represent positive and negative NAO anomaly years, respectively. The dashed lines indicate the boundaries where data points deviate from the mean by ±1 standard deviation.

Table 1 Anomalous years of El Niño–Southern Oscillation (ENSO) and North Atlantic Oscillation (NAO) indices during 1981–2020

Oscillation	Category	Anomalous year
ENSO	Positive years	1983, 1987, 1991, 1992, 1998, 2015, and 2016
	Negative years	1985, 1989, 1996, 1999, 2000, 2008, and 2011
NAO	Positive years	1993, 1994, 2014, 2015, and 2018
	Negative years	1985, 1987, 1996, 2009, and 2010

The Superposed Epoch Analysis (SEA) is widely used to explore the impact of multiple events (Liang et al., 2019; Shi et al., 2021). We performed the SEA on flash drought events in the Qilian Mountains, corresponding to the identified anomalous ENSO and NAO years. During the SEA, data from each positive and negative phase year were aligned with the onset of the respective events. To ensure the robustness and statistical significance of the analysis, we conducted a *t*-test to determine whether the observed variability was significantly linked to ENSO or NAO events, rather than attributable to random fluctuations. Ultimately, the SEA results allow us to comprehensively discuss the different mechanisms by which the positive and negative ENSO and NAO phases influence flash drought events in the Qilian Mountains, illuminating the potential roles of these climate modes in either triggering or mitigating flash droughts across the region.

2.6 Wavelet coherence

Wavelet coherence is an analytical method that utilizes wavelet transforms to identify localized correlations between two time series, and it is particularly suitable for the analysis of non-stationary signals (Lee et al., 2016). We detect dependencies between signals by calculating coherence in both the time and frequency domains, providing insights into the degree of correlation at specific frequencies or scales and how this relationship evolves over time. The key features of wavelet coherence are time frequency localization, allowing localized correlations to be uncovered in certain periods and at specific frequencies, and multiscale analysis, enabling the simultaneous examination of dependencies ranging from short-term fluctuations to long-term trends.

2.7 Integrated Vapor Transport (IVT)

The IVT quantitatively characterizes the intensity and direction of atmospheric water vapor flux, which is characterized by combining wind speed and specific humidity. We performed a vertical integration of the atmospheric moisture flux throughout the entire atmospheric column to construct composite fields of moisture transport under the climatological mean state and different ENSO phases. Subsequently, we analyzed the spatial differences between the composite moisture transport fields during different ENSO phases and the climatological mean state. By incorporating atmospheric circulation patterns, we further explored the modulation effects of different ENSO phases on moisture transport in the study region. The IVT is calculated as follows (Lavers and Villarini, 2013):

$$\mathrm{IVT}=\sqrt{\left(\frac{1}{\mathrm{g}}\int_{\mathrm{surface}}^{\mathrm{top}} qudp\right)^2+\left(\frac{1}{\mathrm{g}}\int_{\mathrm{surface}}^{\mathrm{top}} qvdp\right)^2}, \tag{6}$$

where g is the standard gravitational acceleration constant on the Earth; q is the specific humidity, defined as the mass ratio of water vapor to moist air (kg/kg); u and v are the zonal and meridional wind velocity components, respectively (m/s); and p is the atmospheric pressure (Pa), integrated vertically from the surface (p_{surface}) to the top of the atmosphere (p_{top}).

3 Results

3.1 Temporal variation of flash droughts

Heatwave-induced flash droughts in the Qilian Mountains during 1981–2020 exhibited marked interannual and decadal fluctuations (Fig. 4). A 10-a low-pass filter of the frequency of annual heatwave-induced flash drought events showed higher frequencies during the late 1990s and early 2010s. Conversely, the early 2000s and other intervals contained fewer occurrences of such droughts. There was no statistically significant correlation between the frequency of heatwave-induced flash droughts and warm-season (April–September) mean temperature changes (r=0.230, P=0.180) in the Qilian Mountains (Fig. 4a and c). This suggested that heatwave-induced flash droughts were not solely driven by temperature; other climatic factors (e.g., precipitation and wind speed) may be important. However, short-term temperature increases could exacerbate droughts during specific periods, particularly the late 1990s and early 2010s when heatwave-induced flash droughts occurred more frequently.

Water scarcity-induced flash droughts in the Qilian Mountains during 1981–2020 also exhibited significant interannual and decadal fluctuations (Fig. 4b). From 1981 to approximately 2000, water scarcity-induced drought events increased in frequency. However, after 2000, the frequency began to decrease; this trend was particularly evident from 2010 onwards. Notably, we identified a significant negative correlation (r= –0.388, P=0.018) between water scarcity-induced flash droughts and total precipitation (Fig. 4b and d). Specifically, between 1990 and 2000, the increase in frequency of water scarcity-induced droughts strongly coincided with a decrease in warm-season total precipitation. After 2010, as total annual precipitation increased, the frequency anomaly of water scarcity-induced flash drought events gradually decreased.

3.2 Spatial variation of flash droughts

Accumulated episodes of heatwave-induced flash drought exhibited significant spatial variability, characterized by fewer events in the central and eastern parts of the region, more events in the western part of the region, and increased frequency along the southern edges of the region (Fig. 5a). The spatial variability of accumulated episodes of water scarcity-induced flash drought was less pronounced, with a general pattern of more events in the central and eastern parts of the region, fewer in the western part of the region, and higher frequencies around the periphery compared with the central part of the region (Fig. 5b). The Theil-Sen median trend analysis and MK trend test indicated that heatwave-induced flash drought events significantly increased in the

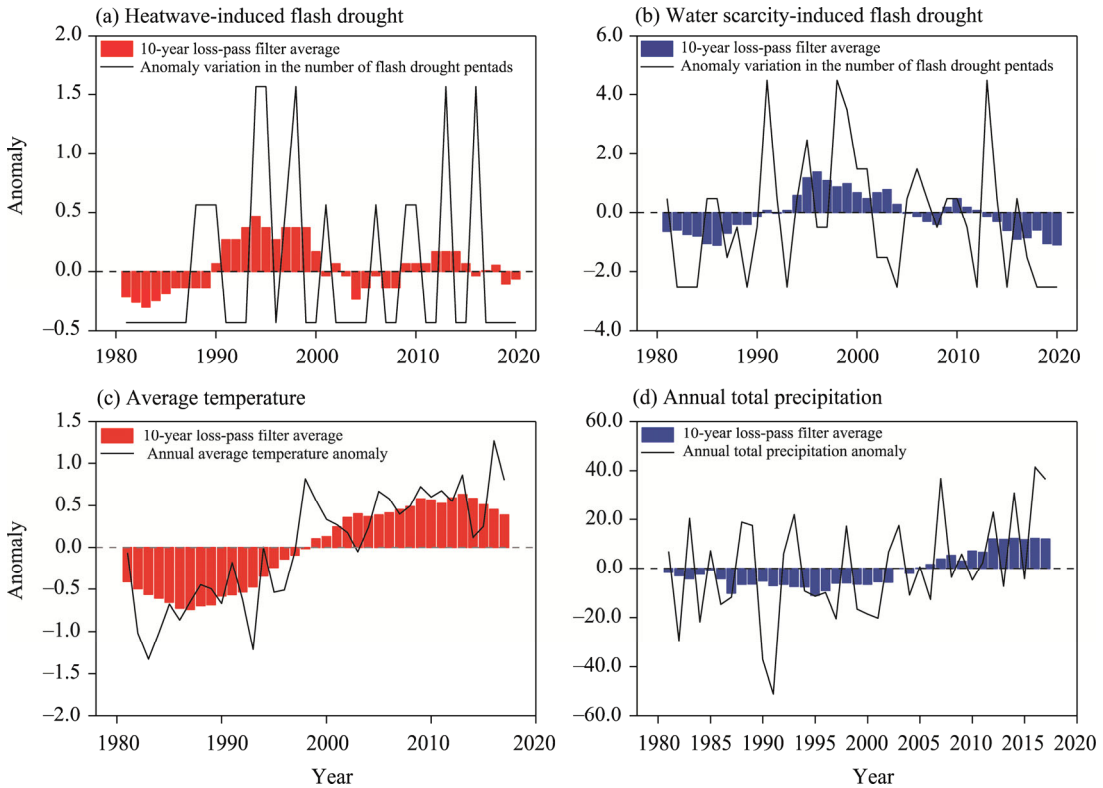

Fig. 4 Interannual and decadal changes in heatwave-induced (a) and water scarcity-induced (b) flash drought events during 1981–2020, and interannual and decadal changes in annual average temperature (c) and annual total precipitation (d) during 1981–2017

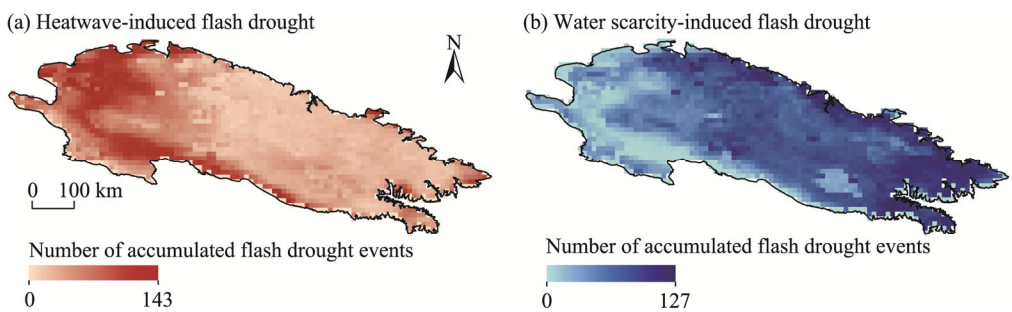

Fig. 5 Spatial distributions of heatwave-induced (a) and water scarcity-induced (b) flash drought events in the Qilian Mountains during 1981–2020

central and eastern parts of the region, significantly decreased in the western part of the region, and remained stable (increase trends were not significant) across other areas during 1981–2020 (Fig. 6a). Temporal trend analysis revealed that water scarcity-induced flash drought events significantly increased in the eastern part of the region during the study period, with those in most other areas remaining no significant increase (Fig. 6b).

3.3 Responses of flash droughts to anomalous ENSO and NAO events

We selected anomalous ENSO and NAO years for composite analysis. We found that at the 95% confidence level, the composite mean values (i.e., composite mean of the time series for abnormal years with different phases of the two atmospheric modes) of water scarcity-induced flash droughts during ENSO positive phases and NAO positive phases, along with heatwave-induced flash droughts during ENSO negative phases, were significantly anomalous (Table 2).

Subsequently, we conducted a composite analysis of the concept series for flash drought events in anomalous years and tested their anomalies.

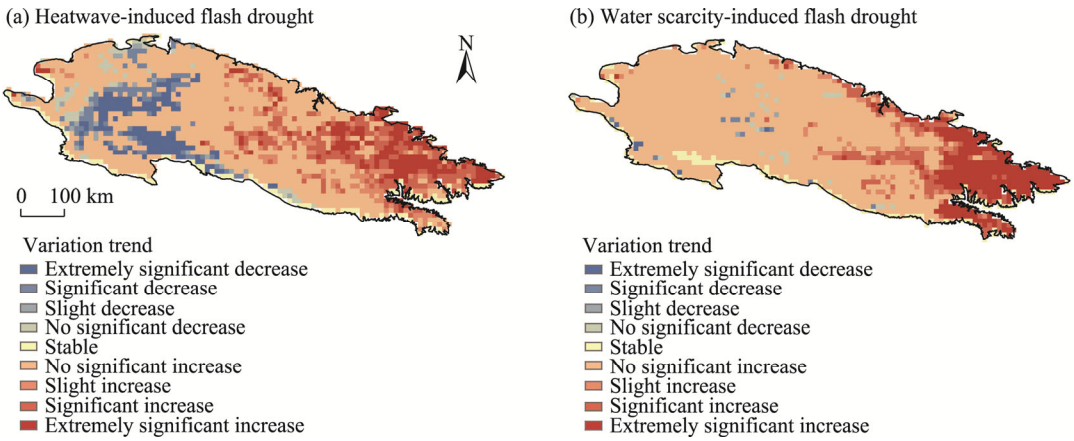

Fig. 6 Variation trend of spatial distributions of heatwave-induced (a) and water scarcity-induced (b) flash drought events in the Qilian Mountains during 1981–2020

Table 2 Anomaly testing for anomalous years of the ENSO and NAO

Condition	Type of drought event	Composite mean value	Confidence interval (95%)	Significant
ENSO positive phase	Heatwave-induced flash drought	0.1366	–0.2061–0.2366	False
ENSO positive phase	Water scarcity-induced flash drought	0.4783	–0.8376–0.4441	True
ENSO negative phase	Heatwave-induced flash drought	–0.2919	–0.2061–0.2366	True
ENSO negative phase	Water scarcity-induced flash drought	0.1925	–0.8376–0.4441	False
NAO positive phase	Heatwave-induced flash drought	–0.0348	–0.2061–0.2366	False
NAO positive phase	Water scarcity-induced flash drought	–1.3217	–0.8376–0.4441	True
NAO negative phase	Heatwave-induced flash drought	–0.0348	–0.2061–0.2366	False
NAO negative phase	Water scarcity-induced flash drought	–0.1217	–0.8376–0.4441	False

Wavelet coherence analyses indicated significant correlations between the temporal variability of flash droughts in the Qilian Mountains and the ENSO and NAO changes at the interannual timescale (Fig. 7). Phase dynamics between the ENSO and NAO indices and the two types of flash drought events were observed across different interannual cycle lengths.

Specifically, the ENSO exhibited a significant in-phase relationship with both types of flash drought events at interannual timescales (1.0–4.0 a) during 1990–2010. This period aligned with the coherence peaks during positive and negative phase years of the ENSO, including 1983, 1987, 1991, 1992, and 1998, suggesting that the ENSO activity in these years may have directly influenced the corresponding periods of heatwave-induced and water scarcity-induced drought events. The impact of the NAO on the two types of drought events exhibited a more complex phase relationship. During 1981–2020, the NAO exhibited an out-of-phase relationship with the two types of flash drought events at 2.0–6.0 a timescale, but an anti-phase relationship at 4.0–6.0 a timescale. Moreover, a significant in-phase relationship occurred between water scarcity-induced droughts and the NAO at a cyclicity of 6.0–8.0 a. These phase differences indicated that positive and negative phase years of the NAO, including 1985, 1987, 1993, 1994, 1996, 2009, 2010, 2014, 2015, and 2018, may have influenced the spatiotemporal distributions of flash drought events in this region.

Anomalous ENSO events, through a series of complex oceanic and atmospheric interactions, may profoundly affect temperature and precipitation within the Qilian Mountains (Fig. 8). An El Niño phase typically brings a warm and moist climate, while a La Niña phase may lead to dryer

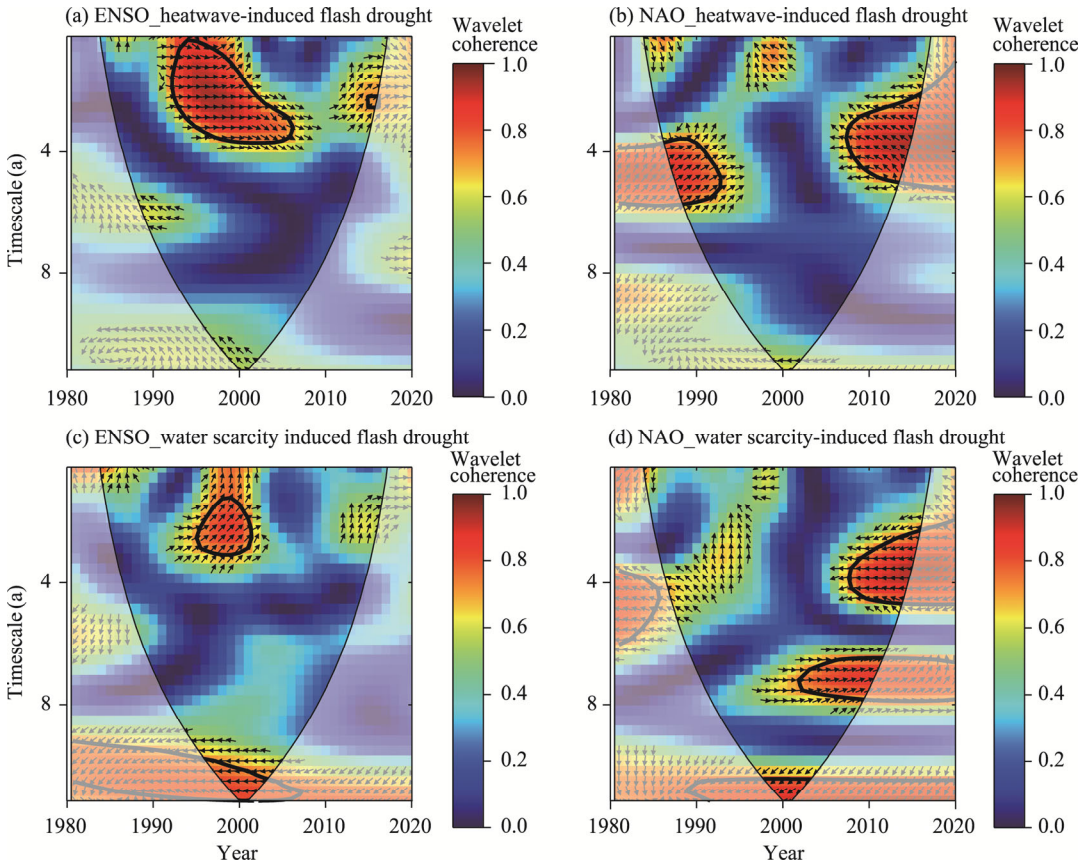

Fig. 7 Wavelet coherence analysis between the frequencies of heatwave-induced and water scarcity-induced flash drought events and the ENSO (a and c) and NAO (b and d) indices. Black arrows represent the phase relationships at designated frequencies and temporal coordinates, where the orientation of the arrows indicates whether the relationship is synchronous, antiphase, or exhibits phase advancement or delay. A black line indicates that the red noise test was passed at the 95% confidence level.

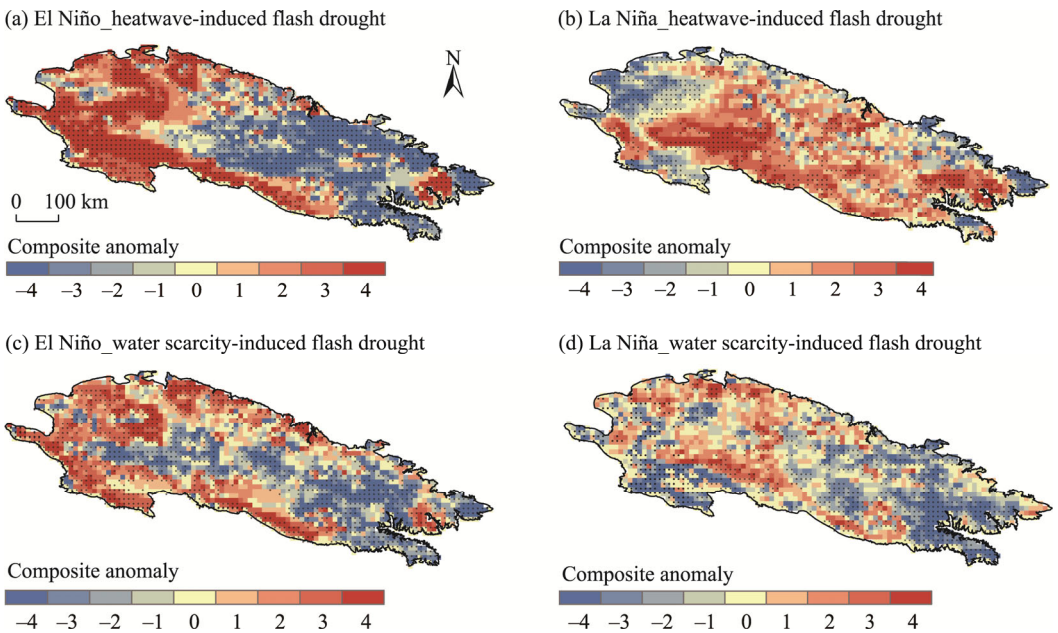

Fig. 8 Responses of occurrence anomalies of heatwave-induced (a and b) and water scarcity-induced (c and d) flash drought events during anomalous years to different phases of the ENSO. *, significance at $P<0.05$ level.

and cooler conditions. During El Niño episodes, heatwave-induced flash droughts were commonly observed along the western and southern fringes of the Qilian Mountains, where a significant heatwave effect occurred, with 70.50% of the grid cells passing the 0.05 significance test (Fig. 8a). In contrast, a lesser number of water scarcity-induced flash droughts were observed during this phase, especially in the central and eastern parts of the region, with 57.42% of the grid cells meeting the same significance criterion (Fig. 8c). However, during La Niña episodes, both heatwave-induced and water scarcity-induced flash drought events recorded limited and spatially dispersed distributions, with 40.16% and 44.08% of grid cells, respectively, passing the 0.05 significance test (Fig. 8b and d).

Variations in positive and negative phases of the ENSO typically lead to anomalous sea surface temperature fluctuations in the tropical Pacific region, enhanced convection, and increased cyclone activity, which, in turn, alter atmospheric circulation patterns. These changes affect the intensity of the Walker Circulation, resulting in shifts in the Asian monsoon system, which subsequently influences moisture transport to the Qilian Mountains.

During El Niño events, circulation changes induced by anomalous sea surface temperature increases in the central and eastern tropical Pacific weaken the Walker Circulation. This, in turn, further enhances the intensity of Asian monsoon systems, especially the East Asian monsoon, allowing warm and moist airflows from the South China Sea and Indian Ocean to be transported to the Qilian Mountains (Fig. 9a), thereby alleviating growing-season drought conditions. Concurrently, precipitation brings a certain evaporative cooling effect. Evaporation removes a part of heat from the air, which mitigates the likelihood of droughts in the eastern and central parts of the region. However, the moist airflows brought by the East Asian monsoon weaken markedly as they reach the western part of the region; here, there is insufficient rainfall to alleviate the high temperatures, leading to the frequent occurrence of both heatwave-induced and water scarcity-induced flash droughts.

In contrast, during La Niña events, anomalously low sea surface temperatures in the central and eastern tropical Pacific strengthen the western branch of the Walker Circulation; this shift leads to a weakening of the East Asian monsoon, hindering the transport of warm and moist air masses to the Qilian Mountains (Fig. 9b), meaning that both types of flash drought events are generally infrequent. Simultaneously, owing to the higher altitudes in southern part of the region, cold and dry airflows extending eastwards from northern areas contribute to a reduction in heatwave-induced flash drought events, particularly in northern and western parts of the region.

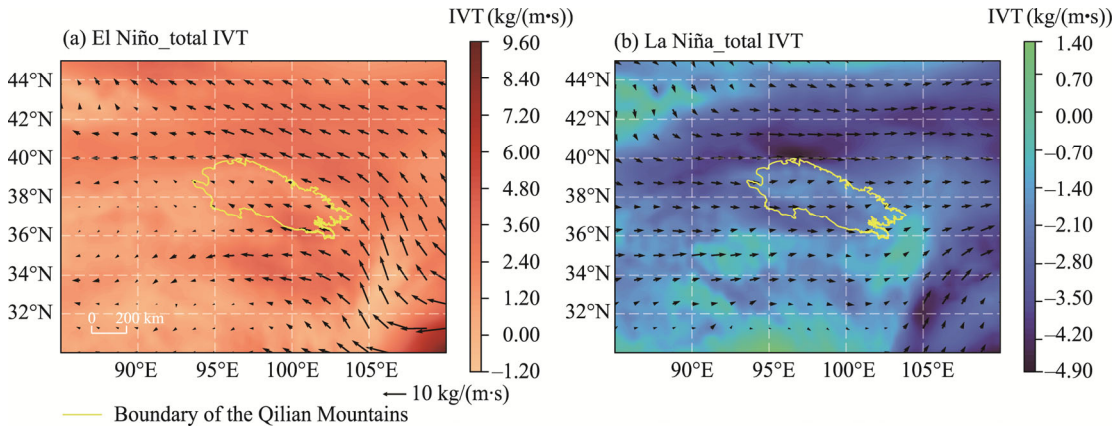

Fig. 9 Composite analysis of moisture flux under positive (a) and negative (b) phases of the ENSO. Arrows indicate the vector field of vapor transport, representing the direction and intensity of the water vapor flux. IVT, integrated vapor transport.

Changes in the westerlies induced by different NAO phases have profound impacts on heat and moisture transport to the Qilian Mountains (Fig. 10). During positive NAO phases,

heatwave-induced and water scarcity-induced flash droughts occurred extensively throughout the Qilian Mountains. Except for a few areas in the east, most of the region experienced a high frequency and intensity of such drought events. Approximately 92.23% and 77.64% of grid cells passed the 0.05 significance test for heatwave-induced and water scarcity-induced flash droughts, respectively (Fig. 10a and c). Negative NAO phases had less impact on flash droughts in the Qilian Mountains. Apart from in the central area, the occurrence of heatwave-induced flash droughts was less frequent across the region, and water scarcity-induced flash droughts were more frequent in the east than in the west, with only 32.38% and 28.93% of the grid cells passing the 0.05 significance test, respectively (Fig. 10b and d).

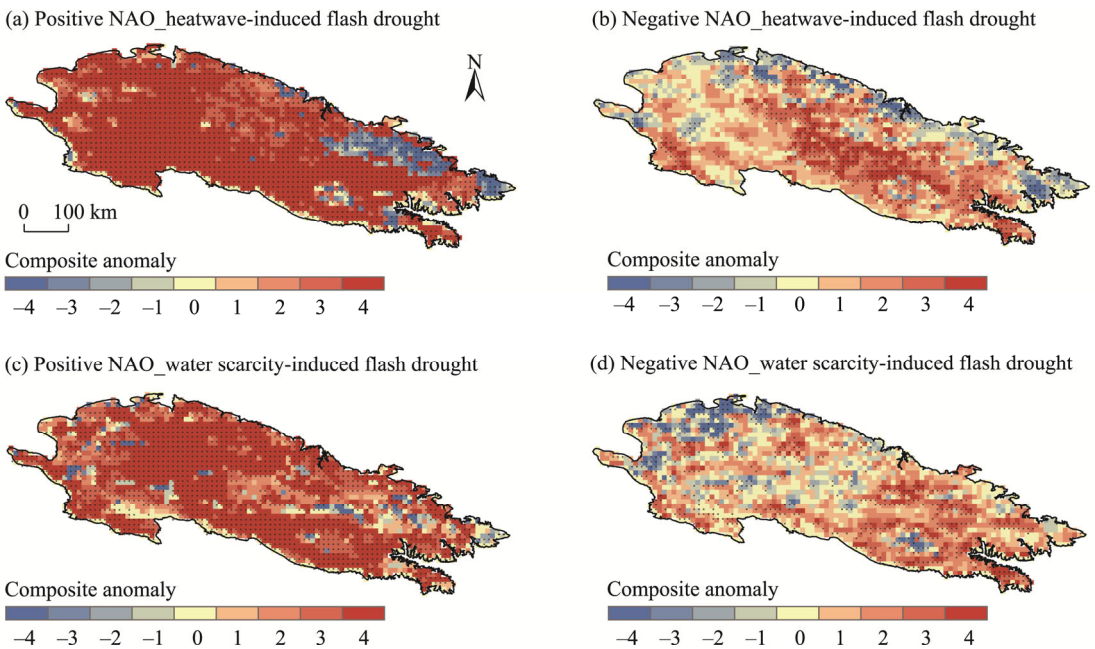

Fig. 10 Occurrence anomalies of heatwave-induced (a and b) and water scarcity-induced (c and d) flash drought events in response to anomalous years of the NAO. *, significance at $P<0.05$ level.

Variations in positive and negative phases of the NAO are associated with abnormal changes in the westerlies in mid-latitudes of the Northern Hemisphere. During a positive NAO phase, the westerlies intensify and the anticyclonic circulation strengthens, resulting in descending air flows. This abnormal subsidence reduces convective activity, weakening precipitation and cloud formation processes. This, in turn, increases surface solar radiation and ground heating. Ultimately, this might increase the probabilities of heatwave-induced and water scarcity-induced flash droughts across the Qilian Mountains region. During a negative NAO phase, the high-pressure system over the North Atlantic weakens, resulting in a corresponding weakening of the westerlies. The weakened westerly flow allows cold air from the Arctic and Siberia to move southwards more easily into inland areas of Europe and Asia, including the Qilian Mountains. This southward-moving cold air remains cool when it reaches the Qilian Mountains during summer, leading to local reductions in temperature and relatively cool conditions; this reduces the occurrence of heatwave-induced flash droughts in the northern part of the Qilian Mountains. However, owing to the high topography, the cold air cannot continue to move southwards, thus limiting its influence on the central and southern parts of the region. Furthermore, the interaction of southward-moving cold air with westerly flows favors precipitation, increasing the likelihood of rainfall in lower-altitude areas of the northwestern Qilian Mountains. Overall, however, owing to the lack of moisture input, most parts of the Qilian Mountains experience reduced precipitation, meaning that water scarcity-induced flash drought events are more likely to occur.

4 Discussion

In this study, we investigated the spatiotemporal variations of heatwave-induced and water scarcity-induced flash droughts occurred in the Qilian Mountains region and explored their relationships with the ENSO and NAO. We found that the temporal variations of these two types of flash drought events exhibit a certain degree of correlation with the overall trends of temperature and precipitation in the Qilian Mountains. Heatwave-induced flash droughts may be closely linked to regional-scale temperature changes and the trend of global warming observed in recent decades (Cui et al., 2022). Higher temperatures can increase evaporation rates and reduce soil moisture, leading to more frequent drought occurrence. The observed negative anomalies in the annual frequency of heatwave-induced flash droughts between 2000 and 2010 appear to be related to "warming hiatuses" observed in the Qilian Mountains as well as many other areas of the globe (Kosaka and Xie, 2013). The general reduction in the occurrence of water scarcity-induced flash droughts in this region also corresponds to an overall increase in precipitation in recent decades (Tian et al., 2014; Wang et al., 2018; Bai et al., 2023). This increase in precipitation may have helped to alleviate long-standing drought issues and may have also altered the spatiotemporal distribution of regional water resources to some extent.

The spatial distributions of both types of flash droughts in the Qilian Mountains exhibit significant heterogeneity owing to complex driving factors, including regional climate change, topography, and socioeconomic conditions. The western part of the Qilian Mountains tends to exhibit higher mean annual temperatures (particularly during the boreal spring and summer) and historically reduced summer precipitation compared with the central and eastern parts (Wang et al., 2022). This pronounced east–west climatic gradient is driven by the interaction between the East Asian summer monsoon and complex topography. Orographic lifting of moist air masses along the eastern slopes of the Qilian Mountains enhances adiabatic cooling, resulting in substantial orographic precipitation; meanwhile, the western slopes usually experience a pronounced rain-shadow effect, leading to aridification and elevated temperatures. The inherent aridity of this region has coupled with amplified temperature extremes under global warming to exacerbate the frequency and intensity of heatwave-induced flash droughts in the western Qilian Mountains. Additionally, there are spatial differences in water storage among the eastern, central, and western parts of the Qilian Mountains. Although precipitation is more abundant in the east, water storage is relatively low, primarily owing to strong evapotranspiration, large agricultural and domestic water demands, and intense exploitation of urban and rural groundwater (Bai et al., 2023); hence, this area is more prone to water scarcity-induced flash drought events. This finding is consistent with a previous study, in which droughts triggered by soil moisture deficits were found to be frequent and intense in the eastern and central areas of the Qilian Mountains (Yin et al., 2023).

Using wavelet coherence analysis, we found that the temporal variability of flash drought events in the Qilian Mountains exhibits strong periodic interactions with ENSO and NAO variations on interannual timescales. The timescales at which they interact are consistent with previous findings in other regions of China. For example, Xing et al. (2019) found a 24- to 40-month resonance period in Guizhou Province, while Zhou et al. (2021) observed 2.60- to 4.93-a cycles in the Yellow River Basin. However, the interaction cycles between flash drought events and the NAO reported herein deviate slightly from those reported in previous research. For example, Xing et al. (2019) demonstrated that the drought index in Guizhou Province significantly interacted with the NAO at timescales of 2.0–3.0 a. Lu et al. (2022) found that the drought index in Henan Province exhibited resonance cycles with the NAO at timescales of 0.5–2.0 a.

Although the Qilian Mountains are located within the Eurasian continent, far from the Pacific and Atlantic oceans, the effects of the ENSO and NAO on flash droughts in this region remain significant (Wang et al., 2014; Zhou et al., 2021; Cui et al., 2022; Zhang et al., 2022). Compared with negative phases, ENSO and NAO positive phases have a more significant impact on both

types of flash drought events in the Qilian Mountains. The impact of the NAO is more complex than that of the ENSO, as indicated by Ren et al. (2024), potentially inducing more pronounced differences in spatial distribution between the two types of flash drought events.

It should be noted that the mechanisms influencing the distribution of flash drought events in the Qilian Mountains may be intricate and include interactions of multiple factors. Hence, there are notable limitations in our study and some of our findings warrant cautious interpretation. The primary limitation lies in the failure to comprehensively consider all potential limiting factors. For example, we have not fully accounted for the regulatory effects of persistent snow cover and permafrost in the natural environment. Herein, the definition of a flash drought event involved a relatively simplified treatment of soil moisture data, neglecting the spatial distribution characteristics of persistent snow cover and permafrost in the Qilian Mountains and their regulatory effects on soil moisture dynamics. As one of the most prominent regions of permafrost on the Xizang Plateau, the permafrost and snow cover system in the Qilian Mountains markedly influence regional climate regulation, hydrological cycles, ecological processes, and human activities (Yang et al., 2010; Wu et al., 2013). Conducting an in-depth investigation of soil moisture characteristics under the influence of permafrost and persistent snow cover in the Qilian Mountains would contribute to a more precise and scientifically robust definition of flash drought events. Moreover, anthropogenic influences, particularly urbanization, may contribute markedly to an increased frequency of extreme temperature events, thereby promoting the occurrence of compound drought events (Tuholske et al., 2021). To further improve the understanding of such extreme drought events, an integrated approach that considers these aforementioned factors is imperative.

5 Conclusions

Using ERA5-Land reanalysis dataset, we examined two types of flash drought events (heatwave-induced and water scarcity-induced flash drought events) in the Qilian Mountains region during 1981–2020. We found that both types of flash droughts have exhibited significant interannual oscillations over recent decades, with a common decadal pattern. These variations were to some extent consistent with observed recent trends in temperature and precipitation variability across the Qilian Mountains region during 1981–2020. Moreover, we revealed that heatwave-induced flash droughts mainly occur in the western Qilian Mountains, while water scarcity-induced flash droughts are more common in the center and east of the region. Both types of droughts have significantly increased in the east of the region during 1981–2020. However, in the western part of the region, heatwave-induced flash droughts have decreased while the frequency of water scarcity-induced flash droughts has remained consistent. Finally, our results suggested that the spatial distributions of flash droughts in this region are significantly associated with anomalous ENSO and NAO events. Compared with the negative phases, the positive phases of ENSO and NAO have a stronger impact on flash drought occurrences in the Qilian Mountains. Moreover, the influence of the NAO is more extensive and complex than that of the ENSO. The findings deepen the mechanistic understanding of drought dynamics in the Qilian Mountains and also provide scientific references for characterizing regional responses to climate change.

Conflict of interest

The authors declare that they have no known competing financial interests or personal relationships that could have appeared to influence the work reported in this paper.

Acknowledgements

This study was supported by the National Natural Science Foundation of China (42477481, 42477483), the Science and Technology Program in Gansu Province (23JRRA599), and the Chinese Academy of Sciences (CAS) "Light of West China" Program.

Author contributions

Conceptualization: WANG Jianglin, BAI Junhong; Data curation: BAI Junhong; Methodology: BAI Junhong; Formal analysis: BAI Junhong; Writing - original draft preparation: BAI Junhong; Writing - review and editing: WANG Jianglin, CHEN Jie, WANG Xuejia; Funding acquisition: WANG Jianglin, WANG Xuejia; Supervision: WANG Jianglin. All authors approved the manuscript.

References

Adib A, Soleimani M, Ashrafi S M, et al. 2024. Monitoring annual meteorological drought in arid and semi-arid watersheds by SPI12 drought index and spatial autocorrelation pattern analysis: A case study of the Khuzestan Province, Southwest Iran. Sustainable Water Resources Management, 10(5): 160–186.

Alizadeh M R, Adamowski J, Nikoo M R, et al. 2020. A century of observations reveals increasing likelihood of continental-scale compound dry-hot extremes. Science Advances, 6(39): eaaz4571, doi: 10.1126/sciadv.aaz4571.

Ayugi B, Eresanya E O, Onyango A O, et al. 2022. Review of meteorological drought in Africa: historical trends, impacts, mitigation measures, and prospects. Pure and Applied Geophysics, 179(4): 1365–1386.

Bai B, Yue P, Zhang Q, et al. 2023. Changing characteristics of ecosystem and water storage under the background of warming and humidification in the Qilian Mountains, China. Science of the Total Environment, 893: 164959, doi: 10.1016/j.scitotenv.2023.164959.

Chen H C, Jin F F. 2020. Fundamental behavior of ENSO phase locking. Journal of Climate, 33(5): 1953–1968.

Cui X, Xu G, He X F, et al. 2022. Influences of seasonal soil moisture and temperature on vegetation phenology in the Qilian Mountains. Remote Sensing, 14(15): 3645, doi: 10.3390/rs14153645.

Dai A, Zhao T B, Chen J. 2018. Climate change and drought: a precipitation and evaporation perspective. Current Climate Change Reports, 4(3): 301–312.

Diffenbaugh N S, Singh D, Mankin J S, et al. 2017. Quantifying the influence of global warming on unprecedented extreme climate events. Proceedings of the National Academy of Sciences, 114(19): 4881–4886.

Dogar M M, Sato T. 2018. Analysis of climate trends and leading modes of climate variability for MENA Region. Journal of Geophysical Research: Atmospheres, 123(23): 13074–13091.

Fu K Q, Wang K C. 2022. Quantifying flash droughts over China from 1980 to 2017. Journal of Geophysical Research: Atmospheres, 127(24): e2022JD037152, doi: 10.1029/2022JD037152.

Gazol A, Camarero J J. 2022. Compound climate events increase tree drought mortality across European forests. Science of the Total Environment, 816: 151604, doi: 10.1016/j.scitotenv.2021.151604.

Gong Z H, Zhu J, Li T T, et al. 2022. The features of regional flash droughts in four typical areas over China and the possible mechanisms. Science of the Total Environment, 827: 154217, doi: 10.1016/j.scitotenv.2022.154217.

Güçlü Y S. 2020. Improved visualization for trend analysis by comparing with classical Mann-Kendall test and ITA. Journal of Hydrology, 584: 124674, doi: 10.1016/j.jhydrol.2020.124674.

Hamed K H, Ramachandra Rao A. 1998. A modified Mann-Kendall trend test for autocorrelated data. Journal of Hydrology, 204(1–4): 182–196.

Hoover D L, Hajek O L, Smith M D, et al. 2022. Compound hydroclimatic extremes in a semi-arid grassland: Drought, deluge, and the carbon cycle. Global Change Biology, 28(8): 2611–2621.

Hu J Y, Yao X J, Zhang C, et al. 2024. Spatial and temporal changes of glaciers and glacial lakes in the northern Tianshan Mountains over the past 30 years. Journal of Geographical Sciences, 34(9): 1857–1880.

Huang L X, Chen J, Yang K, et al. 2023. The northern boundary of the Asian summer monsoon and division of westerlies and monsoon regimes over the Tibetan Plateau in present-day. Science China Earth Sciences, 66(4): 882–893.

Jackson R B, Mooney H A, Schulze E D. 1997. A global budget for fine root biomass, surface area, and nutrient contents. Proceedings of the National Academy of Sciences, 94(14): 7362–7366.

Jiang W G, Yuan L H, Wang W J, et al. 2015. Spatio-temporal analysis of vegetation variation in the Yellow River basin. Ecological Indicators, 51(4): 117–126.

Kosaka Y, Xie S P. 2013. Recent global-warming hiatus tied to equatorial pacific surface cooling. Nature, 501(7467): 403–407.

Lan Y C, Ding Y J, Ersi K, et al. 2003. The relationship between ENSO cycle and temperature, precipitation and runoff in the Qilian Mountain area. Journal of Geographical Sciences, 13(3): 293–298.

Lavers D A, Villarini G. 2013. The nexus between atmospheric rivers and extreme precipitation across Europe. Geophysical Research Letters, 40(12): 3259–3264.

Lee H F, Zhang D D, Pei Q, et al. 2016. Demographic impact of climate change on northwestern China in the late imperial era.

Quaternary International, 425: 237–247.

Li Y, Zheng Z C, Qin Y C, et al. 2021. Relative contributions of natural and man-made factors to vegetation cover change of environmentally sensitive and vulnerable areas of China. Journal of Cleaner Production, 321: 128917–128930.

Li Y, Peng S M. 2023. Ecological and hydrologic evolution history in the sensitive zone of both East Asian summer monsoon and Westerly since the Last Glacial Maximum. Journal of Mountain Science, 20(5): 1266–1281.

Liang E, Dawadi B, Pederson N, et al. 2019. Strong link between large tropical volcanic eruptions and severe droughts prior to monsoon in the central Himalayas revealed by tree-ring records. Science Bulletin, 64(14): 1018–1023.

López-Moreno J I, Vicente-Serrano S M. 2008. Positive and negative phases of the wintertime North Atlantic Oscillation and drought occurrence over Europe: A multitemporal-scale approach. Journal of Climate, 21(6): 1220–1243.

Lu J Q, Gan R, Yang F, et al. 2022. Drought characteristics and its correlation with circulation index in Henan Province based on SPEI index. China Rural Water and Hydropower, 4: 17–24. (in Chinese)

Ma F, Yuan X. 2025. The propagation from atmospheric flash drought to soil flash drought and its changes in a warmer climate. Journal of Hydrology, 654: 132877, doi: 10.1016/j.jhydrol.2025.132877.

Mishra A K, Singh V P. 2010. A review of drought concepts. Journal of Hydrology, 391(1–2): 202–216.

Mo K C, Lettenmaier D P. 2015. Heat wave flash droughts in decline. Geophysical Research Letters, 42(8): 2823–2829.

Neelam M, Hain C. 2024. Global flash droughts characteristics: onset, duration, and extent at watershed scales. Geophysical Research Letters, 51(10): e2024GL109657, doi: 10.1029/2024GL109657.

Nogués-Bravo D, Araújo M B, Errea M P, et al. 2007. Exposure of global mountain systems to climate warming during the 21st Century. Global Environmental Change, 17(3–4): 420–428.

O S, Park S K. 2024. Global ecosystem responses to flash droughts are modulated by background climate and vegetation conditions. Communications Earth & Environment, 5(1): 88, doi: 10.1038/s43247-024-01247-4.

Ogi M, Tachibana Y, Yamazaki K. 2003. Impact of the wintertime North Atlantic Oscillation (NAO) on the summertime atmospheric circulation. Geophysical Research Letters, 30(13): 2003GL017280, doi: 10.1029/2003GL017280.

Otkin J A, Anderson M C, Hain C, et al. 2013. Examining rapid onset drought development using the thermal infrared-based evaporative stress index. Journal of Hydrometeorology, 14(4): 1057–1074.

Park S, Kang D, Yoo C, et al. 2020. Recent ENSO influence on East African drought during rainy seasons through the synergistic use of satellite and reanalysis data. ISPRS Journal of Photogrammetry and Remote Sensing, 162: 17–26.

Raymond C, Horton R M, Zscheischler J, et al. 2020. Understanding and managing connected extreme events. Nature Climate Change, 10(7): 611–621.

Řehoř J, Brázdil R, Trnka M, et al. 2024. Flash droughts in Central Europe and their circulation drivers. Climate Dynamics, 62(2): 1107–1121.

Ren J X, Wang W G, Wei J, et al. 2024. Spatial and temporal variation of summer compound dry-hot events in China and their relationship with climate modes. China Rural Water and Hydropower, 9: 173–180. (in Chinese)

Seneviratne S I, Corti T, Davin E L, et al. 2010. Investigating soil moisture–climate interactions in a changing climate: a review. Earth-Science Reviews, 99(3–4): 125–161.

Sheffield J, Wood E F, Roderick M L. 2012. Little change in global drought over the past 60 years. Nature, 491(7424): 435–438.

Shenoy S, Gorinevsky D, Trenberth K E, et al. 2022. Trends of extreme US weather events in the changing climate. Proceedings of the National Academy of Sciences, 119(47): e2207536119, doi: 10.1073/pnas.2207536119.

Shi P H, Li Y, Biswas A, et al. 2024. Spatial-temporal evolution and intrinsic drivers of compound drought and heatwave events in mainland China. Science of the Total Environment, 948: 174834, doi: 10.1016/j.scitotenv.2024.174834.

Shi W J, Wang M L, Liu Y T. 2021. Crop yield and production responses to climate disasters in China. Science of the Total Environment, 750: 141147–141157.

Spinoni J, Vogt J V, Naumann G, et al. 2018. Will drought events become more frequent and severe in Europe? International Journal of Climatology, 38(4): 1718–1736.

Svoboda M, LeComte D, Hayes M, et al. 2002. The drought monitor. Bulletin of the American Meteorological Society, 83(8): 1181–1190.

Tabari H, Willems P. 2023. Global risk assessment of compound hot-dry events in the context of future climate change and socioeconomic factors. npj Climate and Atmospheric Science, 6(1): 74–84.

Tian H Z, Yang T B, Liu Q P. 2014. Climate change and glacier area shrinkage in the Qilian Mountains, China, from 1956 to 2010. Annals of Glaciology, 55(66): 187–197.

Tuholske C, Caylor K, Funk C, et al. 2021. Global urban population exposure to extreme heat. Proceedings of the National Academy of Sciences, 118(41): e2024792118, doi: 10.1073/pnas.2024792118.

Vicente-Serrano S M, Aguilar E, Martínez R, et al. 2017. The complex influence of ENSO on droughts in Ecuador. Climate Dynamics, 48(1–2): 405–427.

Wang J L, Yang B, Qin C, et al. 2014. Spatial patterns of moisture variations across the Tibetan Plateau during the past 700 years and their relationship with atmospheric oscillation modes. International Journal of Climatology, 34(3): 728–741.

Wang L Y, Yuan X. 2018. Two types of flash drought and their connections with seasonal drought. Advances in Atmospheric Sciences, 35(12): 1478–1490.

Wang S Z, Liu F G, Zhou Q, et al. 2021. Drought evolution characteristics of the Qinghai-Tibet Plateau over the last 100 years based on SPEI. Natural Hazards and Earth System Sciences Discussions, 73: 1–20.

Wang X J, Pang G J, Yang M X, et al. 2018. Precipitation changes in the Qilian Mountains associated with the shifts of regional atmospheric water vapour during 1960–2014. International Journal of Climatology, 38(12): 4355–4368.

Wang Y H, Li D H, Lu G Y, et al. 2022. Characteristics of climate change and its impacts on water resources in Qilian Mountains, China. Chinese Journal of Applied Ecology, 33(10): 2805–2812. (in Chinese)

Wei S H, Wang X J, Wang K, et al. 2023. Rethinking spatiotemporal variations in air temperature over the Qilian Mountains, western China, from 1979 to 2018. Atmospheric Research, 286: 106671, doi: 10.1016/j.atmosres.2023.106671.

Wu T, Zhao L, Li R, et al. 2013. Recent ground surface warming and its effects on permafrost on the central Qinghai-Tibet Plateau. International Journal of Climatology, 33(4): 920–930.

Xing G J, Cui B F. 2019. Drought characteristics variations and its relationship with atmospheric circulation in Guizhou Province. South-to-North Water Transfers and Water Science & Technology, 17(6): 75–85. (in Chinese)

Xing X Y, Fang X H, Pang D, et al. 2024. Seasonal variation of the sea surface temperature growth rate of ENSO. Advances in Atmospheric Sciences, 41(3): 465–477.

Xue Z Y, Chen Y, Yin Y X, et al. 2024. Spatio-temporal characteristics and driving factors of flash drought in northern China from 1978 to 2020. Global and Planetary Change, 232: 104326, doi: 10.1016/j.gloplacha.2023.104326.

Yang M X, Nelson F E, Shiklomanov N I, et al. 2010. Permafrost degradation and its environmental effects on the Tibetan Plateau: A review of recent research. Earth-Science Reviews, 103(1–2): 31–44.

Yao T T, Liu S X, Hu S, et al. 2022. Response of vegetation ecosystems to flash drought with solar-induced chlorophyll fluorescence over the Hai River Basin, China during 2001–2019. Journal of Environmental Management, 313: 114947, doi: 10.1016/j.jenvman.2022.114947.

Yin X W, Wu Y P, Zhao W Z, et al. 2023. Spatiotemporal responses of net primary productivity of alpine ecosystems to flash drought: The Qilian Mountains. Journal of Hydrology, 624: 129865, doi: 10.1016/j.jhydrol.2023.129865.

Zha X N, Xiong L H, Liu C K, et al. 2023. Identification and evaluation of soil moisture flash drought by a nonstationary framework considering climate and land cover changes. Science of the Total Environment, 856: 158953, doi: 10.1016/j.scitotenv.2022.158953.

Zhang L F, Yan H W, Qiu L S, et al. 2021a. Spatial and temporal analyses of vegetation changes at multiple time scales in the Qilian Mountains. Remote Sensing, 13(24): 5046, doi: 10.3390/rs13245046.

Zhang M J, Cao Q, Zhu F L, et al. 2022. The asymmetric effect of different types of ENSO and ENSO Modoki on rainy season over the Yellow River basin, China. Theoretical and Applied Climatology, 149(3–4): 1567–1581.

Zhang W J, Mao W, Jiang F, et al. 2021b. Tropical Indo-Pacific compounding thermal conditions drive the 2019 Australian extreme drought. Geophysical Research Letters, 48(2): e2020GL090323, doi: 10.1029/2020GL090323.

Zhang Y X, Wang H L, Shao X M, et al. 2024. High-resolution reconstruction of April–September precipitation and major extreme droughts in China over the past ~530 years. Science Bulletin, 69(17): 2756–2764.

Zhao T T G, Xiong S T, Tian Y, et al. 2024. Compound dry and hot events over major river basins of the world from 1921 to 2020. Weather and Climate Extremes, 44: 100679, doi: 10.1016/j.wace.2024.100679.

Zhong Z Q, He B, Wang Y P, et al. 2023. Disentangling the effects of vapor pressure deficit on northern terrestrial vegetation productivity. Science Advances, 9(32): eadf3166, doi: 10.1126/sciadv.adf3166.

Zhou B Q, Zhai P M, Liao Z. 2024. Bivariate attribution of the compound hot and dry summer of 2022 on the Tibetan Plateau. Science China Earth Sciences, 67(7): 2122–2136.

Zhou K, Wang Y M, Chang J X, et al. 2021. Spatial and temporal evolution of drought characteristics across the Yellow River basin. Ecological Indicators, 131: 108207, doi: 10.1016/j.ecolind.2021.108207.

Zou J, Lu N, Jiang H, et al. 2022. Performance of air temperature from ERA5-land reanalysis in coastal urban agglomeration of Southeast China. Science of the Total Environment, 828: 154459, doi: 10.1016/j.scitotenv.2022.154459.

Zscheischler J, Westra S, van den Hurk B J J M, et al. 2018. Future climate risk from compound events. Nature Climate Change, 8(6): 469–477.